ELSEVIER

Materials Science and Engineering A261 (1999) 147–157

MATERIALS SCIENCE & ENGINEERING A

# Microalloying for ductility in molybdenum disilicide

U.V. Waghmare [a,*], V. Bulatov [b], E. Kaxiras [a], M.S. Duesbery [c]

[a] *Department of Physics, Harvard University, Cambridge, MA 02138, USA*
[b] *Department of Mechanical Engineering, MIT, Cambridge, MA 02139, USA*
[c] *Fairfax Materials Research, Inc., 7305 Beechwood Drive, Springfield, VA 22153, USA*

**Abstract**

The effects of substitutional alloying on the ductility of $MoSi_2$ single crystals are studied. Criteria for ductility and brittleness are expressed in terms of surface energies and generalized stacking fault energy surfaces, which are calculated using first principles density functional methods. The results are expressed in terms of a single disembrittlement parameter, based on fracture mechanics theory, which characterizes brittle versus ductile behavior. Substitution of Mo by V, Nb, Tc and Re and substitution of Si by Mg, Al, Ge and P were considered. The effects of substitution of Mo by V or Nb, and substitution of Si by Mg or Al are found to be particularly beneficial to the enhancement of ductility. 

*Keywords:* Substitutional alloying; Molybdenum disilicide; Ductility

## 1. Introduction

Molybdenum disilicide crystallizes in an ordered body centered tetragonal structure with $a = 0.320$ nm and $c = 0.785$ nm, formed by alternate stacking of single Mo and double Si (001) layers, as shown in Fig. 1(a). With its high-temperature ductility and exceptional resistance to corrosion and fatigue crack growth, $MoSi_2$ combines the toughness of a metal with the strength of a ceramic and is a promising candidate to replace nickel alloys in the next generation of high-temperature gas turbines. Unfortunately, it undergoes a ductile–brittle transition (DBT) at 1200°C, with the fracture toughness dropping to 2–3 MPa $m^{1/2}$, well below the minimum of 20 MPa $m^{1/2}$ required for engine applications. This brittleness at low temperature means that $MoSi_2$ must be formed by costly electro-discharge machining and places a severe limitation on its potential technological utility. However, there is a reasonable chance that the DBT in $MoSi_2$ may be manipulated or even eliminated. Many of the slip systems in $MoSi_2$ are ductile and it is only for a stress axis near [001] that a DBT is observed [1]. It is believed that the difficulty of operation of non-basal slip systems, particularly $\{013\}\langle 331\rangle$ (see Fig. 1b), is responsible for the embrittlement.

It is desirable therefore, to alter the properties of $MoSi_2$ in very specific ways. This can be, and has in the past been, attempted by heuristically changing the composition or structure of the material and studying experimentally the effect of these changes. It will be argued in this paper that advances in the theory of bonding in solids, based on quantum mechanical density functional calculations, offer an alternative route which can be used as a cost-effective precursor to experiment. The need, in the case of $MoSi_2$, is for an element or elements which can be introduced at microalloy levels ($< 5\%$) and which will perturb the brittle–ductile behavior in favor of ductility without adversely affecting the advantageous physical properties. While the method of choice would normally be an atomistic calculation, bonding in $MoSi_2$ is known to have hybrid metallic and covalent character [2].

Determination of the effects of alloying on such bonding requires accurate quantum mechanical treatment of the electrons, and generation of reliable interatomic potentials, which are an essential prerequisite to atomistic methods, is impractical[1]. Instead, use is made of recent advances in the theory of dislocation nucleation and mobility which provide approximate links

* Corresponding author.

[1] During the time since this work was begun, several groups have developed empirical interatomic potentials for *monolithic* $MoSi_2$, and these are reported on elsewhere in this volume.

0921-5093/99/$ - see front matter 
PII: S0921-5093(98)01060-0

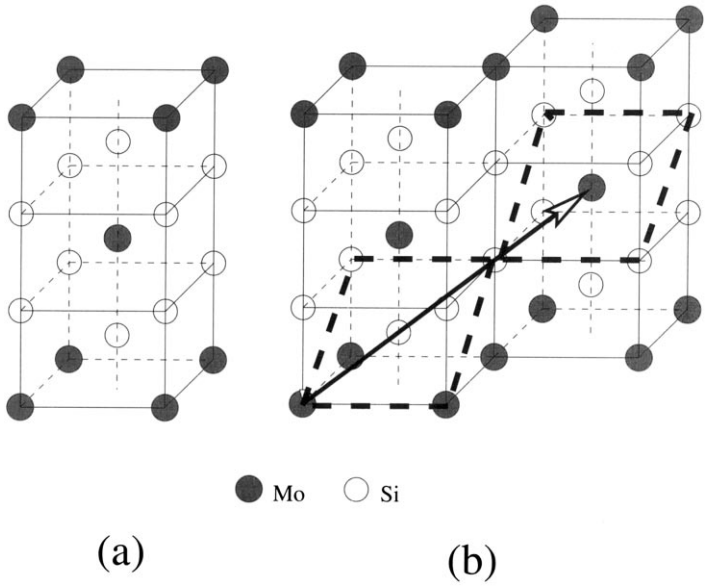


Fig. 1. Crystal structure of $MoSi_2$. (a) Unit cell for the body centered $C11_b$ structure; solid circles represent Mo atoms and open circles represent Si atoms. (b) (013) plane and the Burgers vector for $\{013\}\langle 331\rangle$ slip systems.

between these properties and the generalized stacking fault energy surface, which can be calculated accurately using first principles quantum mechanical techniques. A similar approach has been used successfully by two of the present authors to investigate the DBT in silicon [3]. Even with these gross approximations, the numerical work is intensive. The calculations are restricted to small supercells, with correspondingly large alloy content, and the effects of true microalloying must be estimated by interpolation.

An overview of the experimental background will be presented in the next section. In Section 3 the theoretical basis for the methods used will be detailed. The results for monolithic and alloyed $MoSi_2$ will be given in Section 4.1, and Section 4.2, respectively. Finally, Section 5 will summarize the work and its implications.

## 2. Experimental background

The onset of brittleness is usually due to an increased difficulty in dislocation activity (nucleation or mobility) relative to cleavage. That this may be true for at the DBT in $MoSi_2$ is supported by experiment [4], prestraining at 1300°C increases the ductility of polycrystalline $MoSi_2$ at 800°C from 0 to 5%, and at 750°C to 1.5%. Further confirmation comes from single crystal experiments [1], which show that orientations other than [001] are ductile to room temperature. For [001] orientations, plastic deformation occurs on the $\{013\}\langle 331\rangle$ system, with the flow stress on this slip system increasing rapidly as the DBT temperature is approached from above. This suggests that the onset of brittleness in $MoSi_2$ is due to decreased activity of $\{013\}\langle 331\rangle$ dislocations, leaving no means of accommodation for the component of deformation parallel to the *c* axis. On the other hand, for orientations close to [100], slip on the $\{013\}\langle 331\rangle$ system is observed for temperatures as low as 0°C [1], indicating that the governing process for $\{013\}\langle 331\rangle$ slip is strongly orientation dependent [5].

Several attempts to improve the low-temperature fracture toughness of $MoSi_2$ by forming composite or alloyed materials have been made. The addition of ceramic particles or whiskers such as SiC [6], or $ZrO_2$ [7], acts to inhibit fracture and increase the fracture toughness to a level of $\approx 8$ MPa $m^{1/2}$ by pinning, deflecting or shielding the crack front, or by bridging the crack wake. Incorporation of a ductile second phase, such as Mo in $MoSi_2$ [8], and Nb in $Nb_5Si_3$ [9], increases the fracture toughness (up to $\approx 10$ MPa $m^{1/2}$). This is believed to be due to the crack-slowing effects of large matrix-particle interfacial stresses. The addition of C [10], scavenges silica from the grain boundaries, changing the fracture mode from intergranular to transgranular and increasing fracture toughness to 12 MPa $m^{1/2}$. The most effective treatment to date is the addition of a 30% volume fraction of $Si_3N_4$ particles, which eliminates the oxidation (PEST) problem and raises the high-temperature fracture toughness to 15 MPa $m^{1/2}$. The DBT and low-temperature toughness are unaffected [11]. The addition of C-lubricated SiC (SCS-6) continuous fibers increases the fracture toughness [12], to 35 MPa $m^{1/2}$ for cracks normal to the fiber length. Unfortunately, the toughness for cracks running parallel to the fibers is unaffected. This process is costly and not easily extended to three dimensions, making it an unsuitable candidate for practical use.

Several workers have examined the effect of chemical alloying on the DBT in $MoSi_2$. Chin and co-workers [13], from the United Technologies Laboratory, examined a wide range of ternary $MoSi_2$ alloys. They considered the substitution of Al, B and Ge for Si and Hf, Nb and Re for Mo. For substitution of Al at 20 and 50% of the Si sites, the compound structure was the hexagonal C40. B was found to be insoluble. For Ge at 10, 20 and 50% of Si sites, the $C11_b$ structure was maintained. Hf was insoluble. For Nb at 50% Mo sites, the structure changed to C40. For Re at 10, 20 and 50% of Mo sites, the $C11_b$ structure was retained. All ternaries were tested both at room temperature and at high temperature. No significant change in the DBT temperature was found for any of the alloys.

The tetragonal $C11_b$ structure is an ABAB... stacking of identical {110} planes. The related hexagonal C40 structure is an ABCABC... stacking of the same ({0001} in hexagonal indices) planes. The C40 variant has been reported for $MoSi_2$ at high temperatures. The transformation between the two lattices is accomplished by motion of (in $C11_b$ notation) $a/4\langle 111\rangle$ partials on {110} planes. This led to an idea, put forward by Umakoshi et al. [14,15], that phase destabilization—i.e. decreased stacking fault energy—could activate slip of partials on {110} planes and thereby increase ductility. However, the observation of $a/4\langle 111\rangle$ faults in $MoSi_2$ has been questioned by Kad and co-workers [16], their TEM diffraction analysis showed the faults to be $a/6[001]\{001\}$, corresponding to a missing plate of silicon. The question of disembrittlement by phase destabilization therefore remains open.

Single crystal tests were performed by Umakoshi and co-workers [17], on $MoSi_2$ ($C11_b$), on Cr, Ta and $NbSi_2$ (C40), on $Ti_5Si_3$ ($D8_8$), and on Co, $(Co,Ni)Si_2$ (C1). All the C40 structures were found to be ductile at room temperature (Cr the least so). The C1 structures were also ductile, but have low melting points (1300°C). The $C11_b$ and $D8_8$ structures were brittle at low temperatures. The addition of a small amount of Cr (3%) was reported to improve ductility [18]. Ikarashi and Ishizaki [19], aimed at the designed disembrittlement of $Zr_5Si_3$ (16H) by making the bonds more metallic. Their idea was to partially substitute the larger Y for Zr, expecting a larger number of Si to cluster around, thereby making the bonds more isotropic and hopefully more metallic. The material was formed but not tested. The indentation hardness decreased, perhaps indicating greater metallicity.

## 3. Theoretical methods and background

In this section the concept of the generalized stacking fault and its energy surface will be introduced. The dependence of dislocation nucleation and mobility on specific properties of the generalized stacking fault energy ($\gamma$-) surface will also be discussed. Theories of the DBT will be outlined, with an emphasis on how these relate to dislocation nucleation and mobility, and hence to the $\gamma$-surface. Finally, a description of the methods used for the first-principles calculations will be provided.

### 3.1. The generalized stacking fault energy

The concept of the $\gamma$-surface was introduced by Vitek [20], and can be explained briefly as follows. Consider a crystal cut into two halves parallel to the (hkl) plane and suppose that one half is displaced relative to the other by a vector $\boldsymbol{f}$. As this vector is varied to span a unit repeat area in the plane of the cut, the energy $\gamma(\boldsymbol{f})$ of the crystal changes and traces out the $\gamma$-surface, which has units of energy per unit area. If the energy is minimized with respect to relative displacement of the crystal halves normal to the fault plane, the fault is referred to as relaxed. The power of the $\gamma$-surface is rooted in its qualitative capability to link microscopic characteristics with macroscopic properties. For example, it can be used at the atomistic level to predict dislocation core properties [21], and also at the macroscopic scale to determine the stress intensity at which dislocations are nucleated at a crack tip [22]. It is also a fundamental material property which can be calculated from first principles, even for complex materials such as $MoSi_2$.

### 3.2. Dislocation mobility

The Peierls–Nabarro model involves representation of the crystal dislocation as a continuous, planar distribution of infinitesimal dislocations $\rho(x)$. This distribution can be obtained from the displacement field $u(x)$ (via the relation $\rho(x) = \mathrm{d}u/\mathrm{d}x$), which can in turn be determined from the integro-differential equation

$$K\int_{-\infty}^{\infty} \mathrm{d}x' \frac{\mathrm{d}u(x')/\mathrm{d}x'}{(x-x')} = -\nabla(\gamma(u(x))) \quad (1)$$

subject to the normalization condition

$$\int_{-\infty}^{\infty} \frac{\mathrm{d}u(x)}{\mathrm{d}x}\mathrm{d}x = \boldsymbol{b} \quad (2)$$

In these equations $K$ is an elastic constant and $\boldsymbol{b}$ is the Burgers vector of the dislocation. Eq. (1) equates the stress on the lattice at a position $x$ due to the infinitesimal dislocation distribution to the gradient of the $\gamma$-surface. Eq. (2) requires that the total misfit be equal to the Burgers vector. These two equations are solved typically by assuming a series solution [23,24], and performing a least squares fit for the coefficients. The next step is to move this dislocation distribution rigidly through a distance of one atomic spacing and

compute the change in energy as a function of position $x$. This energy is the Peierls energy $W_{PN}(x)$ and its maximum gradient is the Peierls stress for rigid dislocations at zero temperature. While this procedure has drawbacks, it has been shown to predict Peierls stresses larger than but within a factor of three of those determined using full atomistic methods, both for dislocations with planar cores [25–28], and dislocations with narrow cores [29–31]. The principal source of error in the method is the neglect of any change in the distribution $\rho(x)$ with position during motion through the lattice; if this constraint is removed, the agreement with atomistic methods is improved substantially [32].

If a rough approximation to the Peierls stress is adequate, the step in which the distribution is translated through the lattice can be bypassed. It has been shown that for the limit of narrow dislocations, the Peierls stress is given directly by the maximum gradient of the $\gamma$-surface along an extremal path (extremal in the sense of being the lowest energy path consistent with the end-points) over which the displacement vector changes continuously from 0 to $b$ [33].

### 3.3. Theories of the ductile–brittle transition

The distinction between ductile and brittle failure in materials and the transition between the two types of behavior at a critical temperature—the DBT—has eluded explanation for decades, and remains one of the outstanding problems to be solved in the deformation of materials. In recent years, with mounting interest in composite materials and the concomitant complication of heterogeneous interfaces, the DBT has assumed added dimensions and importance. There is general agreement that the fundamental competition between brittleness and ductility takes place close to the crack tip, at which the applied tensile stress is intensified by the lenticular shape of the crack [34]. The competing processes which lead to brittle or ductile behavior are the extension of the crack by creation of fresh surfaces (brittle response) or the generation of dislocations which blunt the crack and/or produce shielding stresses which reduce the stress intensity at the crack tip (ductile response). In the former process, the energy required for an incremental advance in the crack front is

$$G = 2\gamma_s \tag{3}$$

where $G$ is the energy release rate (the elastic energy released per unit area swept by the crack front) and $\gamma_s$ is the surface energy per unit area.

The first attempt to rationalize the distinction between brittle and ductile behavior was made by Kelly and his colleagues [35], who postulated that a material would be ductile if the crack tip stress exceeded the theoretical shear stress before the theoretical tensile stress was reached. A major theoretical advance, this work failed to address the DBT, in which the failure mode changes from brittle to ductile over a temperature range which can be quite small. A direct linkage to the DBT was made by the later model of Rice and Thomson [36] (RT), in which it was proposed that the onset of ductile behavior occurred when spontaneous emission of dislocations from the crack tip became enabled. The emitted dislocations then serve the dual purpose of blunting the crack at an atomic level and of exerting a shielding stress, the net result of both effects being to reduce the stress level at the crack tip. In the RT model, dislocations which propagate more than a critical distance, $r_c$, from the crack tip are repelled by the crack and are therefore considered to be nucleated. If $r_c$ is less than the dislocation core radius, $r_0$, the material is considered to be ductile at all temperatures; on the other hand, if $r_c > r_0$, the material is brittle at low temperatures. The linkage of the RT model to dislocation properties, specifically the dislocation energy, ostensibly introduces a temperature-based DBT. Unfortunately, the RT model predicts large activation energies (equal to the sum of the core and elastic energies of the dislocation) for dislocation nucleation in brittle materials, precluding a DBT at temperatures significantly below the melting point, $T_m$. Experimentally, the DBT is found to occur at much lower temperatures, for example at $2T_m/3$ in Si.

There are three modern theories of the DBT. In a modern variant of the RT model, Rice [22], points out that in order to nucleate a dislocation with Burgers vector $\boldsymbol{b}$, it is necessary to follow the minimum-energy trajectory on the $\gamma$-surface between the points 0 and $b$. This trajectory is the same as the extremal path introduced in the preceding section in connection with the Peierls stress. At some point along this path the energy reaches a maximum, which Rice calls the unstable stacking fault energy, $\gamma_{us}$. This is the dislocation nucleation energy. It is much smaller than the total dislocation energy (the RT nucleation energy), and is of the same order as the surface energy. Within the Rice model, the criterion for dislocation nucleation at the crack tip, and therefore for ductility, is reached when

$$G = \alpha\gamma_{us} \tag{4}$$

where $\alpha$ is a constant which depends on the geometry of the crack, but is of order unity [37]. At this point a direct connection between the unstable fault energy, which is the maximum energy along a particular extremal trajectory on the $\gamma$-surface, and the Peierls stress, which is given approximately by the maximum slope along this same extremal path. Provided that the energy variation along the extremal path is not too far removed from being sinusoidal, a property which is usually the case, the maximum slope of the curve will scale directly with the maximum energy. In other

words, the Peierls stress will scale directly with the unstable fault energy and any change in one of these will be accompanied by a proportional change in the other.

In an alternative model of the DBT, Hirsch and Roberts [38,39] (HR), postulate that the governing mechanism is the motion, rather than the nucleation of dislocations. The crack tip stresses are presumed to activate internal sources, with dislocations of one sign moving into the bulk and of the opposite sign being absorbed into the crack. Absorption of dislocations of one sign is, of course, exactly equivalent to emission of dislocations with the opposite sign. The HR theory therefore connects the DBT with dislocation mobility. This, as shown in Section 3.2, scales approximately with the unstable fault energy.

The final model is due to Khantha, Pope and Vitek [40–42] (KPV), who argue that the shielding dislocations are nucleated in the vicinity of the crack tip as a self-screening cloud of dipoles by a Kosterlitz–Thouless mechanism [43]. In this case the key quantity is the total dislocation energy, as in the RT model. However, the elastic energy term is much smaller due to the smaller screening length of the KPV model. The second term in the total energy, the dislocation core energy, does not scale with the screening length and remains the same as for the RT model. It is precisely this core region in which the misfit assumes the magnitude at which the $\gamma$-surface reaches the unstable fault energy, so that the core energy depends on $\gamma_{us}$. Therefore, although the mechanistic details of KPV are very different from both the Rice and the HR models, $\gamma_{us}$ is a key parameter for the KPV also.

In summary, the conditions for both brittle fracture and the nucleation and motion of dislocations can be expressed in terms of the two energies $\gamma_s$ and $\gamma_{us}$ Brittleness will occur if the condition Eq. (3) is satisfied before Eq. (4); if the converse is true, the material will be ductile. It is convenient to define a disembrittlement parameter $D=\gamma_s/\gamma_{us}$. The value of $D$ that corresponds to the DBT is not known with any precision, but can be estimated to lie between 1 and 10. For present purposes, that is, to assess whether an alloying element enhances or degrades the ductility of $MoSi_2$, it is sufficient to determine whether the dopant increases or decreases the value of $D$ relative to its value in the ideal crystal.

### 3.4. Theoretical methods

The first principles total energy method is based on the local density approximation (LDA) [44,45], to density functional theory (DFT) [46,47]. A pseudopotential approximation is used to represent the ion-electron interaction and a plane wave basis to represent the electronic wavefunctions and charge density. This type of calculation for simple systems such as Si and Al has proven very reliable in the study of structural properties of bulk and surfaces. Optimized pseudopotentials are used [48], for the transition metals (Mo, V, Nb, Tc and Re) with semicore s and p levels treated as valence states. The calculations for the lattice constant and bulk modulus of the bulk elemental crystals and $MoSi_2$ resulted in excellent agreement with experiment. An energy cut-off up to 60 Ry has been used in these calculations to ensure convergence of energy differences within 1 mRy/atom. A Fermi–Dirac broadening scheme with $kT=0.04$ eV is used to represent the Fermi surface discontinuity and 343 $k$-points are used to sample the Brillouin zone of a single unit cell of $MoSi_2$. At an energy cut-off of 60 Ry, a calculation with three formula units of $MoSi_2$ per cell involves finding the lowest 40 eigenstates of a $5000\times5000$ matrix for any given $k$-point. For efficient calculations on metallic systems involving large unit cells and surfaces, a preconditioned conjugate gradient algorithm [49], is used to interactively diagonalize the Kohn–Sham Hamiltonian. The Kerker charge density mixing scheme [50], is used in the self consistent procedure to avoid sloshing of charge between the vacuum and the slab region. This special charge density mixing scheme mixes small wave vector components of the charge density gradually and thereby damps oscillations during the self-consistency cycle. Surface energies $\gamma_s$ are obtained from the difference between the total energy $E_{tot}$ of a crystal cleaved across a given plane and of the bulk. The calculations use periodic boundary conditions. In practice, the total energy of a periodic supercell is calculated as a function of $d$, the distance between two atomic layers of the desired cleavage plane. These energies are fitted to the universal binding energy function [51]:

$$e(d)=\frac{E_{tot}(d)}{A}=e_\infty-2\gamma_s(1+x)e^{-x} \quad (5)$$

where $x=(d-d_{bulk})/\lambda$, $e_\infty$ is the energy per unit area ($A$) of the cleavage plane, $d_{bulk}$ is the interplanar separation in the bulk crystal and $\lambda$ is a length scale parameter.

The unstable stacking fault energy is obtained from the total energy of a supercell containing the cut plane and with atoms on either side of the plane displaced with respect to each other in the direction of the fault vector.

## 4. The projected influence of microalloying on ductility

### 4.1. The properties of monolithic $MoSi_2$

The $MoSi_2$ unit cell, as can be seen in Fig. 1, is formed by the alternate stacking of single Mo and

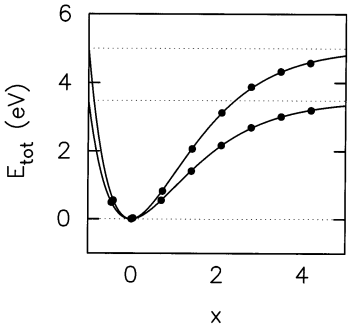


Fig. 2. First principles energies (points) fit to the universal equation of state (solid lines), for pure Mo–Si (open circles) and Si–Si (filled circles) cleavage planes of $MoSi_2$; $x$ is the distance between the two adjacent atomic layers in units of the length scale parameter $\lambda$.

double Si (001) layers. Both types of atom are highly coordinated, with ten nearest neighbors, and as expected at this coordination level, $MoSi_2$ is metallic. Brittle failure in single crystals occurs only when the stress axis is close to [001] and is caused by increasing difficulty in operation of the $\langle 331\rangle\{013\}$ slip system. To assess ductility trends, 75 for (001) cleavage planes and $\gamma_{us}$ for the $\langle 331\rangle\{013\}$ slip system have been calculated from first principles. In $MoSi_2$, there are two types of (001) cleavage planes, one separating adjacent layers of Si atoms and another separating layers of Mo and Si atoms. A supercell consisting of six (001) atomic layers (conventional tetragonal unit cell with two $MoSi_2$ formula units) has been used in the calculation of $\gamma_s$. Fig. 2 shows the total energies for the two (001) surfaces fitted to Eq. (5). The energies in the limit of infinite interplanar separation with respect to the minimum (bulk energy) give the surface energies. The results show that binding between (001) Si planes ($\gamma_s = 2.74$ J m$^{-2}$) is weaker than that between (001) Mo and Si planes ($\gamma_s = 3.94$ J m$^{-2}$). Since the surface relevant to brittle failure is that with the smaller $\gamma_s$, the focus in the alloy calculations below will be on the energetics of cleavage between (001) silicon planes. To obtain a microscopic picture of bonding and better understanding of the above results, contour plots of the electronic charge densities in various planes of $MoSi_2$ have been generated. The contours range from the highest density (due to the contribution from core 4s and 4p electrons), at Mo atoms (the large open circles), to the lowest at Si atoms (the small open circles). Fig. 3(a) shows plots of the electronic charge density in a (110) plane, which contains all the bonds that are broken in a (001) cleavage. There is directional bonding between nearest neighbor Mo and Si atoms appearing as triangular (anisotropic) regions, indicating covalent character. In contrast, there is no significant bonding between Si–Si and Mo–Mo atoms. This naturally results in lower cleavage energies for the (001) planes that separate Si-planes. The charge densities in (001) planes

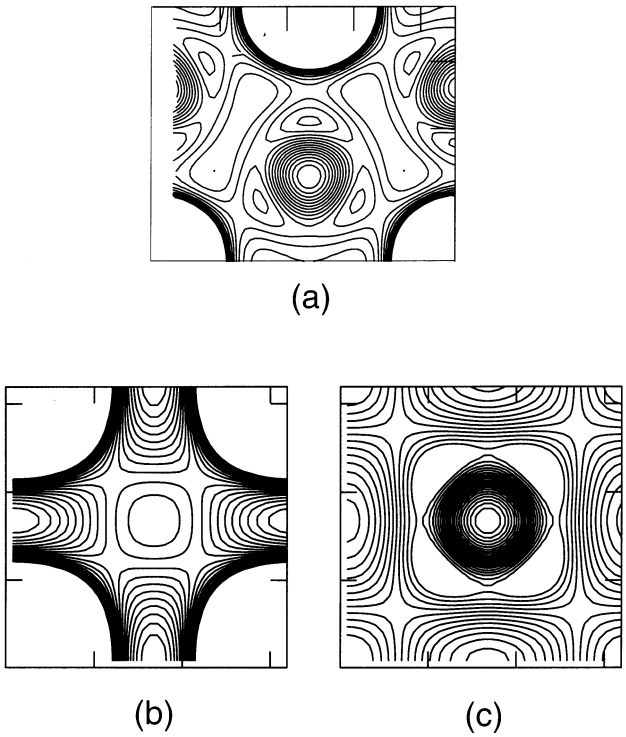


Fig. 3. Electronic charge densities of $MoSi_2$ in (a) the (110) plane, (b) the (001) plane of Mo atoms, and (c) the (001) plane of Si atoms. Red color corresponds to large and purple to small charge densities. Mo atoms are at the center of circular red regions in (a) and (b), and Si atoms are at the center of circular black regions in (a) and (c).

are shown in Fig. 3(b and c). For both Mo (Fig. 3b) and Si (Fig. 3c) (001) layers, the charge densities are close to being isotropic. In addition, the small variation in charge density of Si layers indicates metallic character. The atomic arrangement in the (013) plane is shown in Fig. 4(a), with the two smallest Burgers vectors, $\boldsymbol{b}_0 = 1/2[131]$ and $\boldsymbol{b} = 1/2[331]$. This plane is treated as a basal plane of a supercell used in the calculation of the stacking fault energy surface. For a few points on the $\gamma$-surface, supercells with two and three (013) atomic planes were used also, to check convergence of the results with respect to supercell size. All the results for the $\gamma$-surface presented here have been obtained with calculations for a 3-layer supercell, shown in Fig. 4(b). Fig. 5 shows cross-sectional branches of the $\gamma$-surface along the two possible Burgers vectors. For the slip systems $\langle 131\rangle\{013\}$, and $\langle 331\rangle\{013\}$, respectively, the unstable fault energies are 4.33 and 2.99 J m$^{-2}$. This means that nucleation of dislocations on the latter system is energetically favored, despite the higher energy of dislocations with the $\langle 331\rangle$ Burgers vector (the energy of a dislocation is approximately proportional to the square of its Burgers vector). The intermediate energy minima along these curves indicate possible stable stacking faults. Connection of these results to

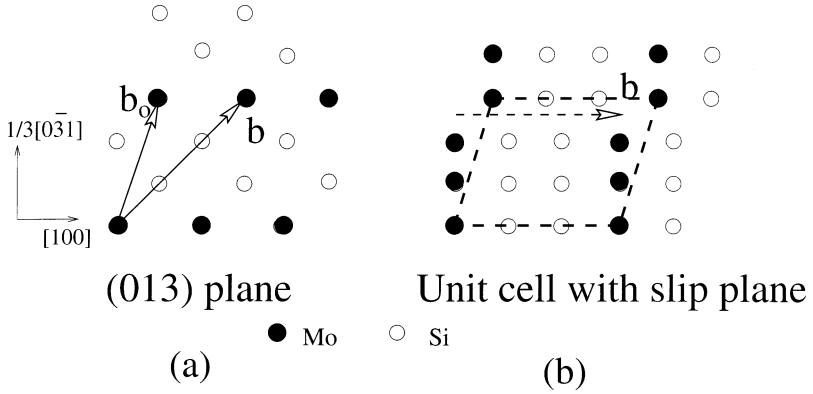


Fig. 4. (a) Atomic arrangement in the (013) plane and the two smallest Burgers vectors. (b) Schematic geometry of the 3-layer supercell (side-view) used in the calculation of generalized fault energies. The dashed arrow indicates displacement of the upper half relative to the lower half of the crystal along a Burgers vector. The thick dashed line indicates the boundary of the supercell corresponding to a finite relative translation of the two halves.

possible dislocation dissociation and anti-phase boundary faults in $MoSi_2$ is the subject of a separate publication [52].

### 4.2. The properties of microalloyed $MoSi_2$

In the preceding section, the properties of the cleavage and slip systems relevant to the DBT in $MoSi_2$ were determined, using a combination of first principles calculations and experimental information. To study the effects of substitutional alloying on ductility, the surface and unstable stacking fault energies for these planes were calculated, using ordered supercells with a few of the Si or Mo atoms replaced by alloying elements. The goal was to examine the effects of a specific alloying element on the bonding in $MoSi_2$ through changes produced in the disembrittlement parameter $D$. First, the effects of Al substitution for Si were examined. A single (001) plane of silicon atoms was replaced by aluminum and the surface energies for various (001) planes were calculated. The results are shown schematically in Fig. 6. For most of the (001) cleavage planes, $\gamma_s$ decreases with Al substitution. Effects on the $\gamma_s$ for cleavage at Si–Si planes are much stronger than those for cleavage at Mo–Si planes. These effects are strongly localized, decaying rapidly with distance normal to the plane of Al substitution. The electronic charge densities for Al-substituted $MoSi_2$ are shown in Fig. 7. The concentrations of 50% (Fig. 7a) and 100% (Fig. 7b) planar substitution correspond, respectively, to 16 and 33% by volume, or 4.4 and 8.9% by weight. Comparison with the ideal $MoSi_2$ crystal, shown in Fig. 7(c), reveals that the changes in charge densities are localized near the plane of Al substitution. These effects become stronger with concentration. The bonding of Si atoms in the plane of substitution with neighboring atoms gets substantially reduced, so that the value of $\gamma_s$ near these planes is more severely affected than for other planes. The unstable stacking fault energies for Al-substituted $MoSi_2$ are obtained by replacing half or all of the Si atoms in the operative {013} slip plane. With 100% planar substitution (33% by volume) of aluminum for

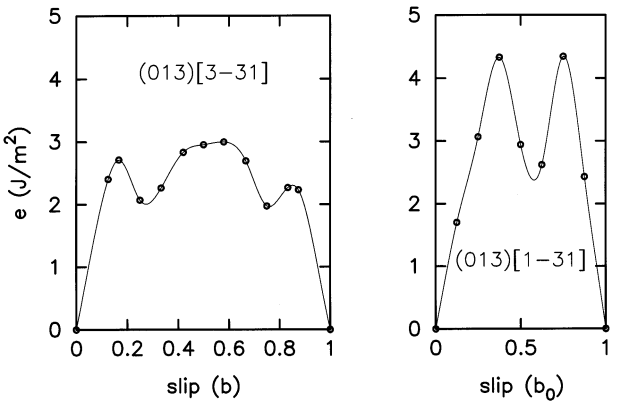


Fig. 5. Cross-sections along ⟨131⟩ and ⟨331⟩ (corresponding to the two vectors shown in Fig. 4(a) of the {013} $\gamma$-surface of $MoSi_2$.

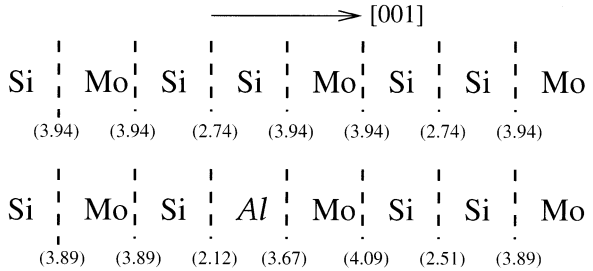


Fig. 6. Schematic representation of the $MoSi_2$ crystal. Each element symbol represents an entire (001) plane of atoms of this type, while the dashed lines represent cleavage planes. The numbers in parentheses are the calculated surface energies $\gamma_s$ for cleavage on those planes. The representation and numbers at the bottom are for a crystal with an entire Si plane near the middle of the slab substituted by Al.

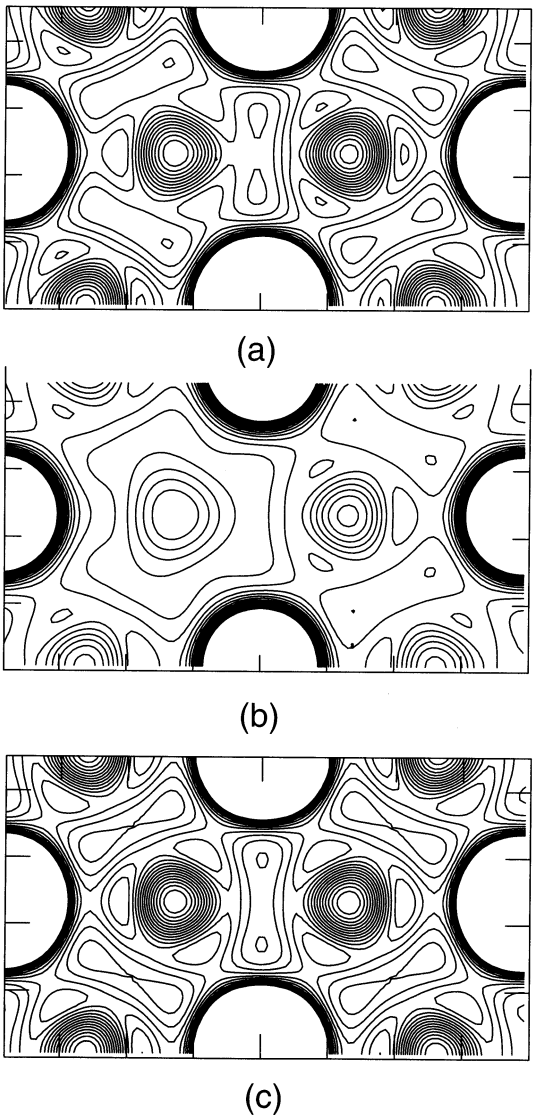


Fig. 7. Electronic charge densities on the (110) plane of Al-substituted $MoSi_2$ with (a) 50% and (b) 100% planar substitution (Al atoms are substituted in the third atomic layer from top indicated by an arrow). For reference, (c) shows the charge density of monolithic $MoSi_2$.

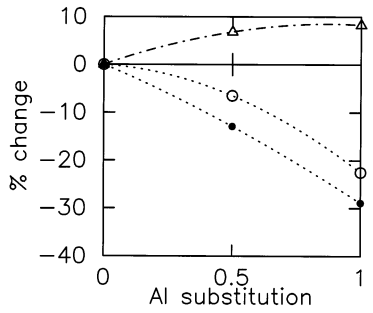


Fig. 8. Percentage reduction in $\gamma_s$ (open circles) and $\gamma_{us}$ (closed circles) and percentage change in $D$ (open triangles) as a function of planar concentration of Al substitution. The lines connecting these points are guides to the eye.

Table 1
Effects on $\gamma_s$ and $\gamma_{us}$ of full planar substitution of Si by Mg, Al, Ge and P[a]

| Element | $\gamma_s$ ($Jm^{-2}$) | $\gamma_{us}$ ($Jm^{-2}$) | $(D-D_0)/D_0$ |
|---|---|---|---|
| Si | 2.74 | 2.99 | 0.00 |
| Mg | 1.61 | 1.45 | 0.21 |
| Al | 2.12 | 2.13 | 0.08 |
| Ge | 2.32 | 3.05 | −0.17 |
| P | 1.78 | 2.58 | −0.26 |

[a] $D$ is the disembrittlement parameter and $D_0$ its value for the ideal crystal ($D_0 = 0.92$).

silicon, $\gamma_{us}$ is reduced by 29%. These calculations did not include atomic relaxation. To estimate the effects of relaxation, a configuration corresponding to a maximum in the $\gamma$-surface was permitted to relax. While the atomic relaxation reduced $\gamma_{us}$ by 12–20%, the percentage reduction in $\gamma_{us}$ (relative to its value in the ideal crystal) due to Al-substitution remained essentially unchanged. The change with concentration of the effects of Al-substitution on $\gamma_s$ and $\gamma_{us}$ were also examined. These quantities were calculated for 0 (pure $MoSi_2$), 50 and 100% planar concentrations of Al, and the results are shown in Fig. 8. The reduction in $\gamma_{us}$ (shown in Fig. 8 as filled circles) varies nearly linearly with Al concentration. The percentage reduction in $\gamma_{us}$ is larger than that in $\gamma_s$ for all the concentrations considered, particularly for small concentrations. Hence the disembrittlement parameter $D$ is increased as shown in Fig. 8. A more limited investigation was conducted into the effects of substitution of Mg, Ge and P for silicon. The results for $\gamma_s$ and $\gamma_{us}$ with full planar substitution are summarized in Table 1. It is found that both $\gamma_s$ and $\gamma_{us}$ decrease for substitution by Mg and P. For Ge, $\gamma_s$ decreases but $\gamma_{us}$ increases slightly. Overall, the disembrittlement parameter $D$ decreases with the number of valence electrons in the substituted element, indicating that alloying with acceptor elements should be better for the enhancement of ductility than alloying with isoelectronic or donor elements. Additional results (Fig. 9) for $\gamma_{us}$ for substitution with these elements at 50% substitution reveal that, to a good approximation, $\gamma_{us}$ varies linearly with concentration in all cases. Finally

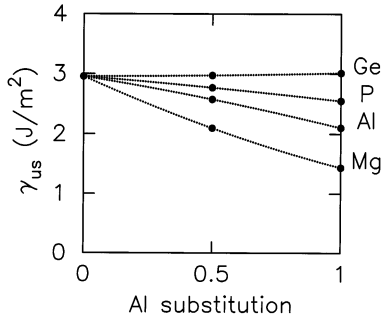


Fig. 9. $\gamma_{us}$ as a function of planar concentration of Mg, Al, Ge and P, substituted for Si. The lines connecting these points are guides to the eye.

the effects of substituting V, Nb, Tc and Re for Mo were explored. The results for $\gamma_s$ and $\gamma_{us}$ are presented in Table 2. As we have shown above, brittle failure involves the breaking of Si–Si bonds only; therefore substitution for Mo has little effect on $\gamma_s$. On the other hand, strong Mo–Si bonds are broken during dislocation nucleation, and hence any substitution for Mo which weakens these bonds should and does lead to a reduction in $\gamma_{us}$ comparable to that found in the substitution for Si. The disembrittlement parameter $D$ increases with V, Nb and Tc substitutions, although, as for Si-substitution, the effect is weaker for the alloying element with a higher valence charge. $D$ decreases slightly with substitution of Re for Mo, suggesting that alloying with Re is likely to embrittle $MoSi_2$ rather than improve the ductility. The effects of V and Nb substitution on $D$ are very similar, because of their same valence. Fig. 10 shows the charge densities in (110) planes for the cases of 50% V and Tc substitution and compares them to the ideal $MoSi_2$ crystal charge density. In contrast with the substitutions for Si, the effects of Mo-substitution on charge density are more long-ranged. The covalent nature of Mo–Si bonds persists, but is somewhat weaker. This is consistent with the small changes in $\gamma_s$ found with these substitutions. The effect of V substitution for Mo on the bonds with nearest neighbor Si atoms is found to be stronger than that of Tc substitution for Mo.

## 5. Discussion and conclusions

The interpretation of macroscopic mechanical properties such as ductility and brittleness in terms of fundamental cohesive properties is a complex and difficult task. The present work uses a highly simplified treatment, which borrows heavily from fracture mechanics and dislocation theory, to make the connection between first principles quantum mechanics and macroscopic properties, and to obtain reliable values for the crucial quantities that enter into the analysis. There has been much work linking first principles results to simpler macroscopic properties (for example the elastic constants) for selected materials. To the authors' knowledge, the present work is the first of its kind in two respects:

- It constitutes the first attempt to use first principles, non-empirical techniques to provide a prescription for the design of materials with better ductility.
- It is the first of its kind to be motivated by a technological imperative, rather than by the cutting edge of scientific capability.

There are many approximations and simplifications which have been made in the approach. For example, it has been assumed that the dopant is soluble in the $MoSi_2$ matrix and that the crystal structure is unaffected by alloying. In a similar vein, sheer numerical complexity mandates the use of small supercells. These

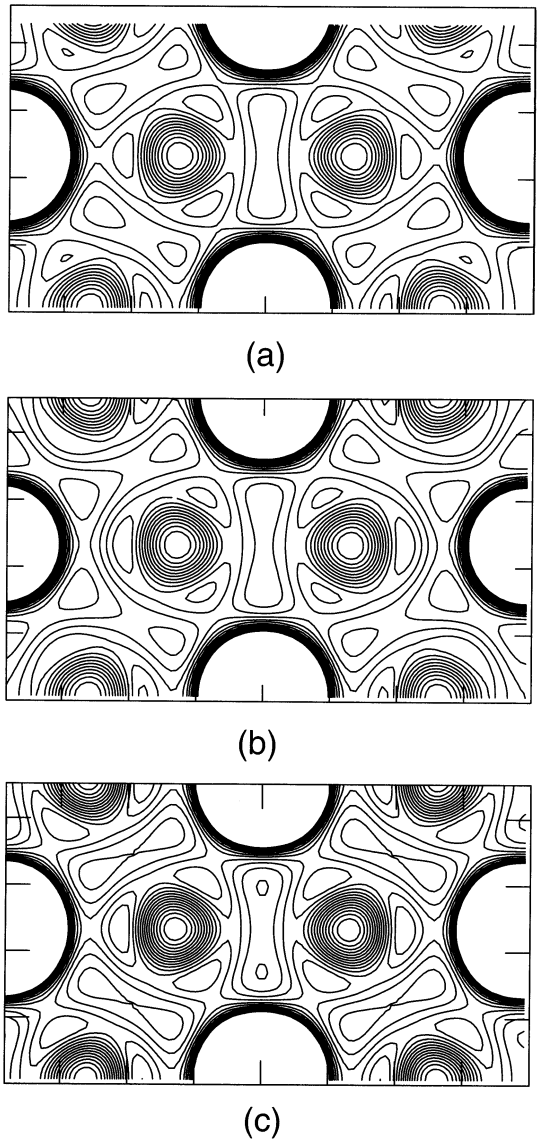


Fig. 10. Electronic charge densities in the (110) plane of (a) V-substituted and (b) Tc-substituted $MoSi_2$ (V and Tc atoms are substituted for Mo atoms in the top and the bottom layers indicated by arrows). For comparison, (c) shows the charge density of monolithic $MoSi_2$.

Table 2
Effects on $\gamma_s$ and $\gamma_{us}$ of full planar substitution for Mo with V, Nb and Tc[a]

| Element | $\gamma_s$ (J m$^{-2}$) | $\gamma_{us}$ (J m$^{-2}$) | $(D-D_0)/D_0$ |
|---|---|---|---|
| Mo | 2.74 | 2.99 | 0.00 |
| V | 2.49 | 2.30 | 0.18 |
| Nb | 2.60 | 2.42 | 0.18 |
| Tc | 2.35 | 2.34 | 0.10 |
| Re | 2.25 | 2.55 | −0.04 |

[a] $D$ is the disembrittlement parameter and $D_0$ its value for the ideal crystal ($D_0 = 0.92$).

correspond to large concentrations, despite the stated intention of looking at the microalloy regime. No attempt will be made to justify these assumptions and approximations. Rather, they are rationalized within the philosophy of providing the best information possible, subject to the twin constraints of technical capability and a real problem. The results show trends for ductility which can be correlated with electronic structure, and which are expected to provide a cost-effective guide to experiment. It is worth noting that the authors were not aware of the recent experimental work [53,54], confirming the predicted breed of increased fracture toughness with aluminum substitution until after the calculations were completed. This experimental confirmation is particularly gratifying in light of the drastic approximations employed.

In conclusion, a simple model for ductile versus brittle response and input from first principles calculations have been used to estimate the effects of substitutional alloying on the ductility of $MoSi_2$, with the object of providing a rational guide for experimental efforts to disembrittle $MoSi_2$ at low temperatures. Within the simplified treatment, it is predicted that a quaternary compound which substitutes small concentrations of Mg or Al for Si and V or Nb for Mo will enhance the ductility of $MoSi_2$ without significantly degrading its desirable physical properties.

## Acknowledgements

This work was performed with support from the Office of Naval Research under SBIR contract no. N000 14-97-C-0104. Some of the calculations were performed using ACRES code developed under the CHSSI project. The authors wish to acknowledge useful discussions with Dr J.J. Petrovic, Dr R.J. Hecht, N. Bernstein, M. Bazant, N.A. Modine, G. Smith and E.B. Tadmor.

## References

[1] K. Ito, H. Inui, Y. Shirai, M. Yamaguchi, Philos. Mag A72 (1995) 1075.
[2] B.K. Bhattacharya, D.M. Bylander, L. Kleinman, Phys. Rev. B 32 (1985) 7973.
[3] E. Kaxiras, M.S. Duesbery, Phys. Rev. Lett. 70 (1993) 3752.
[4] R. Gibala, H. Chang, C.M. Czarnik, MRS Symposium on High Temperature Silicides and Refractory Alloys, Boston, 1993, MRS, Pittsburg, p. 49.
[5] T.E. Mitchell, S.A. Maloy, Critical Issues in the Development of High Temperature Structural Materials, 1993, TMS, Warrendale PA, p. 279.
[6] A.K. Bhattacharya, J.J. Petrovic, J. Amer. Ceram. Soc 74 (1991) 2701.
[7] J.J. Petrovic, R.E. Honnell, T.E. Mitchell, T.E. Wade, K.J. McClellan, Ceram. Eng. Sci. Proc 12 (1991) 1633.
[8] T.C. Lu, A.G. Evans, R.J. Hecht, R. Mehrabian, Acta Metall. Mater. 39 (1991) 1853.
[9] R.M. Nekkanti, D.M. Dimiduk, Mater. Res. Soc. Proc. 194 (1990) 175.
[10] S. Maloy, A.H. Heuer, J.J. Lewandowski, J.J. Petrovic, J. Amer. Ceram. Soc. 1991 (1991) 2704.
[11] M. Hebsur, ONR Workshop on $MoSi_2$, Hyannis, Mass., 1995, unpublished.
[12] S. Rawal, ONR Workshop on $MoSi_2$, Hyannis, Mass., 1995, unpublished.
[13] S. Chin, D.L. Anton, A.P. Giamei, MRS Symposium on High Temperature Silicides and Refractory Alloys, Boston, Mass., 1993, Materials Research Society, Pittsburgh, 1993, p.423.
[14] Y. Umakoshi, T. Sakagami, T. Yamane, T. Hirano, Philos. Mag. Lett. 59 (1989) 159.
[15] Y. Umakoshi, T. Sakagami, T. Hirano, T. Yamane, Acta Metall. Mater. 38 (1990) 909.
[16] B.K. Kad, K.S. Vecchio, B.P. Bewlay, R.J. Asaro, MRS Symposium on High Temperature Silicides and Refractory Alloys, Boston, Mass., 1993, Materials Research Society, Pittsburgh, 1993, p. 49.
[17] Y. Umakoshi, T. Nakashima, T. Nakano, E. Yanagisawa, MRS Symposium on High Temperature Silicides and Refractory Alloys, Boston, Mass., 1993, Materials Research Society, Pittsburgh, 1993, p. 9.
[18] Y. Umakoshi, T. Hirano, T. Sakagami, T. Yamane, TMS Symposium on High Temperature Aluminides and Intermetallics, 1990, TMS, Warrendale, 1990, p. 111.
[19] Y. Ikarashi, K. Ishizaki, MRS Symposium on High Temperature Silicides and Refractory Alloys, Boston, Mass., 1993, Materials Research Society, Pittsburgh, 1993, p. 235.
[20] V. Vitek, Philos. Mag 18 (1968) 773.
[21] M.S. Duesbery, V. Vitek, Acta Mater. 46 (1998) 1481.
[22] J.R. Rice, J. Mech. Phys. Solids 40 (1992) 239.
[23] A.J.E. Foreman, M.A. Jaswon, J.K. Wood, Proc. Phys. Soc. Lond. B64 (1951) 156.
[24] V. Vitek, L. Lejcek, D.K. Bowen, in: P.C. Gehlen, J.R. Beeler, R.I. Jaffee (Eds.), Interatomic Potentials and Simulation of Lattice Defects, Plenum Press, New York, 1972, p. 493.
[25] V. Vitek, M. Yamaguchi, J. Phys. F: Met. Phys. 3 (1973) 537.
[26] M. Yamaguchi, V. Vitek, J. Phys. F: Met. Phys. 3 (1973) 523.
[27] M. Yamaguchi, V. Vitek, J. Phys. F: Met. Phys. 5 (1975) 1.
[28] M. Yamaguchi, V. Vitek, J. Phys. F: Met. Phys. 5 (1975) 11.
[29] B. Jobs, Q. Ren, M.S. Duesbery, Phys. Rev. B50 (1994) 5890.
[30] Q. Ren, B. Joos, M.S. Duesbery, Phys. Rev. B 52 (1995) 13223.
[31] L.B. Hansen, K. Stokbro, B.I. Lundqvist, K.W. Jacobsen, D.M. Deaven, Phys. Rev. Lett. 75 (1995) 4444.
[32] V. Bulatov, E. Kaxiras, Phys. Rev. Lett. 78 (1997) 4221.
[33] B. Joos, M.S. Duesbery, Phys. Rev. Lett. 78 (1997) 226.
[34] C.E. Inglis, Trans. Inst. Naval Arch. 55 (1913) 219.
[35] A. Kelly, W.R. Tyson, A.H. Cottrell, Philos. Mag. 15 (1967) 567.
[36] J. Rice, R. Thomson, Philos. Mag. 29 (1974) 73.
[37] J.R. Rice, G. Beltz, J. Mech. Phys. Solids 42 (1994) 333.
[38] P.B. Hirsch, S.G. Roberts, J. Samuels, Proc. R. Soc. Lond. A421 (1989) 25.
[39] P.B. Hirsch, S.G. Roberts, Philos. Mag. A 64 (1991) 55.
[40] M. Khantha, D.P. Pope, V. Vitek, Phys. Rev. Lett. 73 (1994) 684.
[41] M. Khantha, V. Vitek, Acta Mater. 45 (1997) 4675.
[42] M. Khantha, D.P. Pope, V. Vitek, Acta Mater. 45 (1997) 4687.
[43] J.M. Kosterlitz, D.J. Thouless, J. Phys. C: Solid State Phys. 6 (1973) 1181.
[44] D.M. Ceperley, B.J. Alder, Phys. Rev. Lett. 45 (1980) 566.
[45] J.P. Perdew, A. Zunger, Phys. Rev. B 23 (1981) 5048.
[46] P. Hohenberg, W. Kohn, Phys. Rev. B 136 (1964) 864.
[47] W. Kohn, L.J. Sham, Phys. Rev. A 140 (1965) 1133.

[48] A.M. Rappe, K.M. Rabe, E. Kaxiras, J.D. Joannopoulos, Phys. Rev. B 41 (1990) 1227.
[49] M.P. Teter, M.C. Payne, D.C. Allan, Phys. Rev. B 40 (1989) 1255.
[50] G. Kreese, J. Furthmuller, Comput. Mater. Sci 6 (1996) 15.
[51] J.H. Rose, J.R. Smith, F. Guinea, J. Ferrante, Phys. Rev. B 29 (1984) 2963.
[52] U.V. Waghmare, V. Bulatov, E. Kaxiras, M.S. Duesbery,@ Phil. Mag., (1998), in press.
[53] P. Peralta, S.A. Maloy, F. Chu, J.J. Petrovic, T.E. Mitchell, Scripta Mater. 37 (1997) 1599.
[54] P. Peralta, F. Chu, S.A. Maloy, P. Santiago, J.J. Petrovic, T.E. Mitchell, Computer Aided Design of High-Temperature Materials, Santa Fe, New Mexico, 1997.